Chemistry & Biology, Vol. 12, 1337–1347, December, 2005, ©2005 Elsevier Ltd All rights reserved. DOI 10.1016/j.chembiol.2005.09.017

Chemistry and Biology of Moverastins, Inhibitors of Cancer Cell Migration, Produced by *Aspergillus*

Yasushi Takemoto,[1,4] Hidenori Watanabe,[2,4] Kenji Uchida,[2] Koji Matsumura,[2] Koichi Nakae,[1] Etsu Tashiro,[1] Kazutoshi Shindo,[3] Takeshi Kitahara,[2] and Masaya Imoto[1,*]

[1]Department of Bioscience and Informatics
Faculty of Science and Technology
Keio University
3-14-1 Hiyoshi, Kohoku-ku
Yokohama 223-8522
Japan

[2]Graduate School of Agricultural and Life Sciences
University of Tokyo
1-1-1 Yayoi, Bunkyo-ku
Tokyo 113-8657
Japan

[3]Department of Food and Nutrition
Japan Women's University
2-8-1, Mejirodai, Bunkyo-ku
Tokyo 112-8681
Japan

Summary

Cancer cell migration is a required step in cancer metastasis. We screened for inhibitors of cancer cell migration of microbial origin, and obtained moverastin, a member of the cylindrol family, from *Aspergillus* sp. F7720. However, the results of an NMR spectroscopic analysis raised the possibility that moverastin is a mixture of two diastereomers. Separation of the C-10 epimers of synthetic moverastin and a bioassay revealed that both diastereomers (moverastins A and B) had inhibitory effects on cell migration. Furthermore, we demonstrated that moverastins A and B inhibited FTase in vitro, and they also inhibited both the membrane localization of H-Ras and the activation of the PI3K/Akt pathway in EC17 cells. Thus, moverastins inhibited the migration of tumor cells by inhibiting the farnesylation of H-Ras, and subsequent H-Ras-dependent activation of the PI3K/Akt pathway.

Introduction

Cell migration is a central feature of a range of physiological processes, including embryonic development, tissue repair, and inflammation. Cell migration is a complex, multistep process that involves protrusion of the leading edge of the cell, the formation of adhesion complexes, myosin/actin-mediated cell contraction, and the release of adhesion complexes at the cell's rear. When cells migrate, filopodia and lamellipodia are formed at the leading edge. Filopodia and lamellipodia are made up of actin filaments, and are formed mainly through actin polymerization [1–4]. Consistent with the complexity of the cell migration process, a variety of intracellular signaling molecules and their associated biochemical pathways have been identified in the regulation of this process. The Rho family of small GTPase proteins, including Rho, Rac, and Cdc42, modulates cell migration by affecting the dynamic reorganization of the actin cytoskeleton [5, 6]. Rho regulates the formation of contractile actin-myosin filaments to form stress fibers, while Rac and Cdc42 regulate the formation of lamellipodia and filopodia, respectively [7–9].

Another small GTPase protein, Ras, is also known to make an essential contribution to cell migration in endothelial and fibroblast cells [8, 10–12]. Three members of the Ras family, H-, K-, and N-Ras, are ubiquitously expressed in mammalian cells. Among Ras proteins, the amino-terminal 85 amino acids are identical, and the middle 80 amino acids exhibit 85% homology, while the carboxy-terminal sequences are highly divergent [13].

The biological effects of Ras proteins are exerted through the activation of several downstream effectors. Ras stimulates the serine/threonine kinase Raf, leading to the activation of the downstream kinase mitogen-activated protein kinase (MAPK)/extracellular signal-regulated kinase (Erk) kinase (MEK), which, in turn, phosphorylates Erks/MAPK. Activated Erks/MAPK phosphorylates, and thereby enhances the activity of myosin light chain kinase, resulting in the phosphorylation of myosin light chains and cell migration [14, 15]. Moreover, activated Erks/MAPK accumulates in the nucleus and phosphorylates Elk-1, which results in the expression of several genes, such as matrix metalloprotease (*mmp*)-9; MMP-9 activity is required for the induction of cell motility [16]. In addition to the Raf/MEK/Erk pathway, a phosphoinositide 3-OH kinase (PI3K)/Akt pathway is shown to be critical for the mitogenic and oncogenic effect of Ras. PI3K interacts with Ras and is activated as a result [17–19]. One target of PI3K is serine/threonine kinase Akt. Akt may be regulated by both phosphorylation and by the direct binding of PI3K lipid products to the Akt pleckstrin homology (PH) domain. The PI3K/Akt pathway has been implicated in the regulation of the actin cytosleleton, and is necessary for Cdc42- and Rac-induced cell motility and invasiveness [20].

The Rho family and the Ras family of small GTPases are all modified posttranslationally at their carboxy-termini by isoprenoid lipids. This prenylation through the thiol group of a cysteine side chain near the carboxylate terminus affects the attachment of the GTPase to the plasma membrane, which is crucial to its activation [21]. The isoprenyl substrate for these reactions is either farnesyl pyrophosphate (FPP) or geranylgeranyl pyrophosphate (GGPP), which are derived from mevalonate. Enzymes that catalyze protein prenylation are farnesyltransferase (FTase) and geranylgeranyltransferase (GGTase). FTase catalyzes the farnesylation of proteins with a carboxy-terminal CAAX motif, where C is cysteine, A is an aliphatic amino acid, and X is methionine, serine, glutamine, alanine, or cysteine. Like FTase, GGTase catalyzes the geranylgeranylation of proteins terminating with a CAAX motif, where X is restricted to leucine, isoleucine, or phenylalanine. Among small

*Correspondence: imoto@bio.keio.ac.jp
[4]These authors contributed equally to this work.

GTPase proteins, Ras proteins require farnesylation for their activation. On the other hand, Rho A, Rac, and Cdc42 require geranylgeranylation. Inhibitors of these prenyltransferases, which inhibit the translocation to the plasma membrane and the function of these small GTPase proteins, affect the cytoskeleton and inhibit cell migration [22, 23].

In addition to physiological conditions, cell migration is also involved in pathological conditions, such as metastasis [24, 25]. In metastasis, tumor cells migrate from the initial tumor mass into the circulatory system, which they subsequently leave, migrate into a new site, invade into a tissue compartment, and grow. Thus, the migration of tumor cells is essential for invasion of the extracellular matrix and for cell dissemination. Inhibition of the cell migration involved in the invasion process represents a potential therapeutic approach to the treatment of tumor metastasis. Therefore, we have screened for compounds which inhibit the migration of tumor cells to develop a new antimetastatic drug of microbial origin. In this study, we have obtained moverastin from the culture broth of *Aspergillus* sp. F7720, as a mixture of two diastereomers at the C-10 secondary allylic alcohol. Chemical synthesis and bioassays revealed that both of the C-10 epimers (moverastins A and B) had inhibitory effects on cell migration. Our data suggest that moverastins A and B inhibited the farnesylation of H-Ras, thereby suppressing cell migration in human esophageal tumor cells.

Results

Preparation of the Cell Migration Inhibitor Moverastin from *Aspergillus* sp. F7720

We screened more than 2000 microbial extracts for inhibitors of tumor cell migration by conducting wound healing assays using human esophageal carcinoma EC17 cells, and found activity in the culture broth of a solid-isolated fungal strain, F7720. Since taxonomic studies revealed strain F7720 to belong to *Aspergillus* or a related genus, we named the strain *Aspergillus* sp. F7720. The strain has been deposited in the National Institute of Advanced Industrial Science and Technology, Tsukuba, Japan (Accession No. FERM P-18198). The culture broth (1 liter) was filtered to be separated into a supernatant and a mycelial cake. The supernatant was extracted with EtOAc (1 liter), and evaporated to give a yellow oil (1.52 g). The yellow oil was loaded on a silica gel column, which was eluted with $CHCl_3$-MeOH (100:1). The eluate was concentrated in vacuo, and the yellow powder (37.6 mg) obtained was dissolved in MeOH and was applied to a Sephadex LH-20 column and eluted with MeOH. The active fraction (28.7 mg) was chromatographed on preparative silica gel thin-layer plates (Kieselgel $60F_{254}$; Merck Co., Darmstadt, Germany) using a toluene-acetone (2:1) system. An active band (9.7 mg) thus obtained was further purified by HPLC (Capcell Pak C18 column, 2.0 × 25 cm) with 55% aq acetonitrile to yield moverastin (Figure 1A) as a colorless powder (1.8 mg).

Structural Determination of Moverastin

Moverastin gave an $(M + H)^+$ ion peak at *m/z* 389.2307 in the HRFAB-MS analysis, and its molecular formula was established as $C_{23}H_{32}O_5$ (calculated for 389.2328). In the ^{13}C NMR spectrum of moverastin in $CDCl_3$, some of the signals were observed as two peaks (peak height ratio was approximately 2:1). Considering this observation and the result of HRFAB-MS, moverastin was proposed to be a mixture of two diastereomers (Figure 1A). Since the yield of moverastin was low, and the separation of the diastereomers was difficult, the structure of each diastereomer was analyzed in the mixture. We named the major component moverastin A (**1**) and the minor component moverastin B (**2**).

The ^{13}C NMR spectrum of moverastin A displayed 23 carbons. The C-H COSY spectrum of moverastin A revealed the presence of the following types of carbon: four methyls, five sp^3 methylenes, one exomethylene, three sp^3 methines (one of which was oxygenated), one sp^2 methine, one sp^3 quaternary carbon, six sp^2 quaternary carbons, and two carbonyl carbons (aldehyde and ketone). The ^1H and ^{13}C chemical shifts of moverastin A are listed in Table 1.

Analysis of the ^1H-^1H DQF COSY spectrum of moverastin A gave four partial fragments, as shown by bold lines (Figure 1B), the structural fragments C9 (δ28.53)-C10 (δ76.60), C12 (δ24.87)-C13 (δ35.56), C21 (δ14.96)-C15 (δ36.13)-C16 (δ30.92)-C17 (δ41.54), and C19 (δ50.41)-C22 (δ7.57).

The HMBC experiment was used to assemble these fragments into moverastin A. ^1H-^{13}C long-range correlations from H-8 (δ10.05, aldehyde) to C-1 (δ112.85) and C-6 (δ164.06), and from H-7 (δ2.50) to C-1, C-2 (δ142.65), and C-3 (δ111.98) were observed in the HMBC spectrum. In addition, correlations from H-9 (δ2.89 and δ3.09) to C-4 (δ164.20), C-5 (δ110.32) and C-6, and from H-3 (δ6.32) to C-1 and C-5 were also observed in the HMBC spectrum. From these correlations, the connectivities from C-1 to C-10 (partial structure A in Figure 1B) were clarified. The attachment of an oxygen atom at C-4, C-6, and C-10 was also confirmed by their ^{13}C chemical shifts.

^1H-^{13}C long-range correlations from exomethylene (H-23, δ4.90 and δ5.07) to C-11 (δ150.90) and C-12 (δ24.87) were observed in the HMBC spectrum. Therefore, the presence of C-23–C-11–C-12–C-13 was established (partial structure B in Figure 1B).

The presence of a cyclohexanone structure (partial structure C in Figure 1B) in moverastin A was clarified using the ^1H-^{13}C long-range correlations from H-20 (δ0.61) to C-14 (δ43.48), C-15 and C-19, from H-22 (δ0.93) to C-18 (δ213.77), and from H-17 (δ2.36) to C-18 in the HMBC spectrum.

The connectivities of partial structures A, B, and C were established by the ^1H-^{13}C long-range correlations from H-23 (partial structure B) to C-10 (partial structure A), and from H-20 (partial structure C) to C-13 (partial structure B). The presence of OH at C-4, C-6, and C-10 was determined by elimination. From all the results described above, the planar structure of moverastin A was determined as shown in Figure 1A. Moverastin A is a member of the cylindrol family [26].

The structure of moverastin B was analyzed in the same way, and the planar structure of moverastin B was confirmed to be identical to that of moverastin A. The assigned ^1H and ^{13}C chemical shifts of moverastin B are listed in Table 1. A comparison of ^{13}C chemical

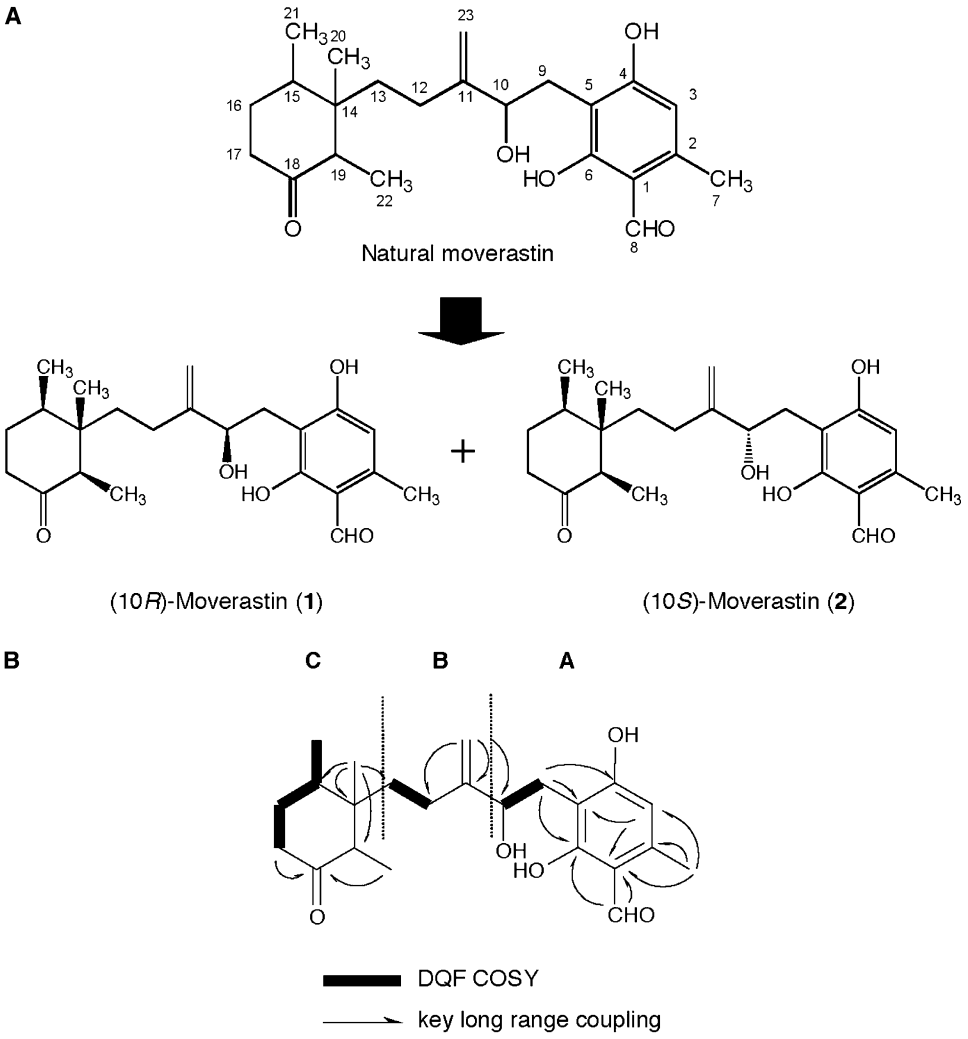

Figure 1. Structural Determination of Moverastin

(A) Structure of moverastin.

(B) HMBC and DQF COSY correlations of moverastin.

shifts between moverastin A and moverastin B was performed, and $|\Delta\delta_C|$ values are shown in Table 1. Considering this result, and the positions of chiral carbons in moverastin A (C-10, C-14, C-15, and C-19), moverastin B was strongly suggested to be the C-10 epimer of moverastin A.

Confirmation of the Structure of Moverastin by the Synthesis of a Mixture of Diastereomers at the C-10 Secondary Allylic Alcohol

To confirm that moverastin is a mixture of the two diastereomers at C-10 ([10*R*]-moverastin [1] and [10*S*]-moverastin [2] in Figure 1A), we synthesized its presumed structure as a diastereomeric mixture (Figure 2). Since the stereochemistries of the three asymmetric centers on the cyclohexanone ring were speculated to be the same as those of other well-known compounds of the cylindrol family based on NMR similarity, we chose ascochlorin (**3**) as the chiral starting material for the left-hand moiety. The ketone of **3** was first protected as a cyclic acetal, and trisubstituted olefin was cleaved selectively by ozonolysis in the presence of pyridine to afford an enone (**5**) via **4** in excellent yield. Hydrogenation of another disubstituted olefin followed by enol-triflation of the methyl ketone (**6**) by Comins' method [27] gave **7** (64% yield), which is a key precursor for the coupling to generate the secondary allylic alcohol. Another right-hand segment for the coupling was prepared starting from known protected orcinol **8** [28]. Ortholithiation at the aromatic carbon between the two MOMO groups and treatment with ally bromide gave **9** in 60% yield. A formyl group was then introduced by treatment with *n*-BuLi and DMF to afford **10** in 54% yield, and subsequent ozonolysis gave dialdehyde (**11**) in 74% yield. Next, a coupling reaction between **7** and **11** was carried out successfully using the Nozaki-Hiyama-Kishi procedure [29, 30], and **12** was obtained in 62% yield as an approximately 1:1 diastereomeric mixture at C-10. In this reaction, nonconjugated aldehyde reacted predominantly, and a coupling product with benzaldehyde was observed only in a trace amount. Finally, acid hydrolysis of ethylene acetal and MOM groups

Table 1. ^{13}C and ^{1}H Data for Moverastin in $CDCl_3$

	δ_H		δ_C		
Position	A	B	A	B	$\Delta\lvert\delta_C\rvert$
1			112.85	112.85	—
2			142.65	142.65	—
3	6.32 (s)	6.32 (s)	111.98	111.98	—
4			164.20	164.20	—
5			110.32	110.23	0.09
6			164.06	164.09	0.03
6-OH	12.84 (s)	12.84 (s)			
7	2.50 (s)	2.50 (s)	18.05	18.05	—
8	10.05 (s)	10.05 (s)	192.84	192.84	—
9	2.89 (dd 7.2, 16.0)	2.85 (dd 7.2, 16.0)	28.53	28.49	0.04
	3.09 (dd 2.0, 16.0)	3.13 (dd 2.0, 16.0)			
10	4.45 (dd 2.0, 7.2)	4.45 (dd 2.0, 7.2)	76.60	76.55	0.05
11			151.01	150.90	0.11
12	1.90–2.00 (m)[a]	1.90–2.00 (m)[a]	24.87	24.98	0.11
	2.20–2.25 (m)[a]	2.20–2.25 (m)[a]			
13	1.40–1.60 (2H, m)[a]	1.40–1.60 (2H, m)[a]	35.56	35.56	—
14			43.48	43.43	0.05
15	2.00–2.10 (m)[a]	2.00–2.10 (m)[a]	36.13	36.13	—
16	1.55–1.65 (m)[a]	1.55–1.65 (m)[a]	30.92	30.95	0.03
	1.85–1.95 (m)[a]	1.85–1.95 (m)[a]			
17	2.35–2.45 (2H)[a]	2.35–2.45 (2H)[a]	41.54	41.54	—
18			213.77	213.77	—
19	2.53 (q 7.2)	2.53 (q 7.2)	50.41	50.41	—
20	0.61 (s)	0.61 (s)	15.38	15.38	—
21	0.90 (d 6.8)	0.91 (d 6.8)	14.96	15.03	0.07
22	0.93 (d 7.2)	0.93 (d 7.2)	7.57	7.52	0.05
23	4.90 (s)	4.90 (s)	108.99	108.77	0.22
	5.07 (s)	5.07 (s)			

Chemical shifts in ppm from TMS as internal standard.
[a] Multiplets with countless peaks are represented by a range of the chemical shift, indicating where the multiplet starts and ends.

afforded a mixture of C-10 stereoisomers of moverastin. The ^{13}C NMR spectrum of the synthetic moverastin showed complete accordance with natural moverastin, including the split peaks, and this result unambiguously showed that natural moverastin is a diastereomeric mixture at C-10.

Preparation of (10*S*)-Moverastin and (10*R*)-Moverastin and Determination of the Absolute Configurations

We then prepared (10*S*)- and (10*R*)-isomers of moverastin to clarify the relationship between bioactivity and stereochemistry at C-10. Since it was found to be difficult to separate both isomers directly, we applied a standard method to the optical resolution of secondary alcohols (Figure 3). The intermediate (**12**) in the synthesis of moverastin was converted into the corresponding (*S*)-α-methoxy-α-trifluoromethylphenylacetate (MTPA ester), and the two isomers were separated by preparative HPLC. Methanolysis of the MTPA ester of each isomer ([10*S*]- and [10*R*]-**13**) and subsequent acid hydrolysis gave (10*S*)- and (10*R*)-moverastin in 61% and 69% yield, respectively. It should be noted that the separation was successful, and no contamination by another stereoisomer was observed in the NMR spectrum of either isomer.

The absolute configurations of the synthetic and natural moverastins were determined as follows. First, (*R*)-MTPA esters of the two separated stereoisomers of **12** were also prepared, and the stereochemistries at C-10 of the two diastereomers were determined by modified Mosher's method [31]. Signs of $\Delta\delta$ values ($\delta_{(S)\text{-MTPA}}$-$\delta_{(R)\text{-MTPA}}$, described at the bottom of Figure 3) of the protons on the right side of MTPAO groups clearly differed from those on the left side, and the stereochemistry at C-10 of each isomer was assigned as depicted in Figure 3. Second, CD spectra of natural moverastin (diastereomeric mixture) and our synthetic (10*S*)- and (10*R*)-moverastins were compared. All of them showed quite similar curves, indicating negative Cotton effects at 290, 286, and 289 nm, respectively. This result suggests that (1) the influence of the asymmetric center at C-10 on CD spectra is very small, (2) their negative Cotton effects depend mainly on the octant rule of the chiral cyclohexanone moiety, and (3) the absolute stereochemistries on the cyclohexanone ring of natural moverastins are the same as those of ascochlorin, which is the starting material of our moverastin synthesis. Finally, by comparing the ^{1}H and ^{13}C NMR spectra of each isomer, moverastin A and moverastin B were identified to be

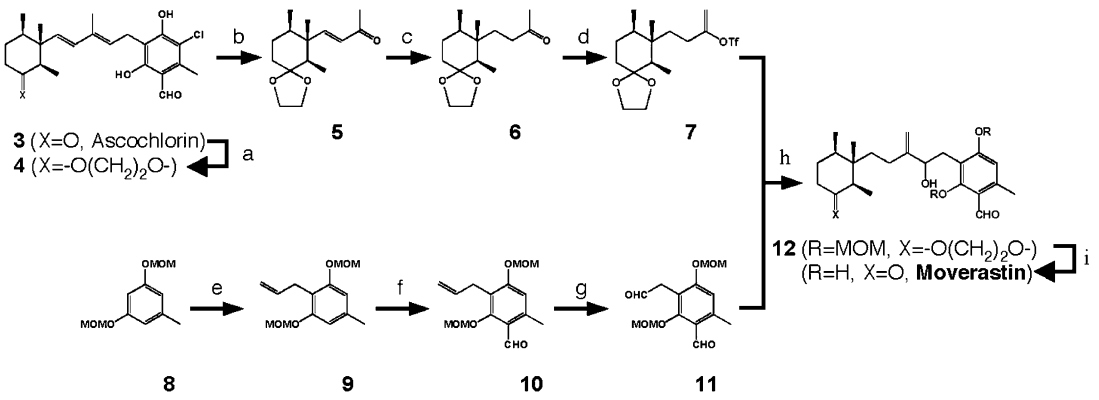

Figure 2. Synthesis of Diastereomeric Mixture of Moverastin

Reagents and conditions: (a) TsOH, $HO(CH_2)_2OH$, toluene reflux (at 70°C), quant; (b) O_3, CH_2Cl_2-pyridine, then Me_2S, 99%; (c) H_2, Pd-C, EtOAc, quant; (d) KHMDS, 5-chloro-2-[*N*,*N*-bis(trifluoromethanesulfonyl)amino]pyridine, THF, −78°C, 64%; (e) *n*-BuLi, CH_2=$CHCH_2Br$, TMEDA, THF, −20°C ~ room temperature, 60%; (f) *n*-BuLi, DMF, TMEDA, ether, −20°C ~ room temperature, 54%; (g) O_3, CH_2Cl_2, then Ph_3P, 74%; (h) $CrCl_2$, $NiCl_2$, DMF, room temperature, 62%; (i) concentrated HCl, THF, room temperature, 82%.

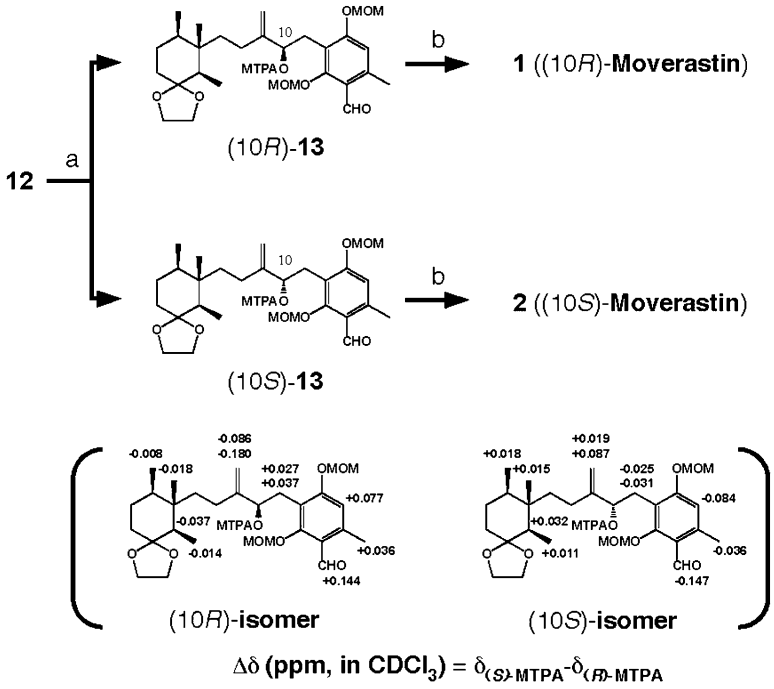

Figure 3. Separation of the Two Diastereomers of Moverastin

Reagents and conditions: (a) (*R*)-MTPACl, DMAP, CH_2Cl_2, room temperature, 81%, then HPLC separation; (b) NaOMe, MeOH, 0°C, then concentrated HCl, THF, 0°C, 69% for (10*R*)-moverastin (**1**), 61% for (10*S*)-moverastin (**2**).

(10*R*, 14*S*, 15*R*, 19*R*)-moverastin (**1**) and (10*S*, 14*S*, 15*R*, 19*R*)-moverastin (**2**), respectively.

Effect of Moverastins A and B on the Migration of EC17 Cells

The inhibitory activities of moverastins A and B were assayed with the wound healing assay, as previously described [32]. As shown in Figure 4A, moverastin A partially inhibited the migration of EC17 cells at 3 μg/ml, and completely inhibited it at 10 μg/ml, as judged from the residual area between the cells inwardly migrating from the edges of the scratch. Moverastin B also inhibited the migration of EC17 cells with the same dose range (Figure 4A). The inhibitory activities of moverastins A and B were reassessed with a chemotaxicell chamber (Figure 4B). In this assay, EC17 cells were cultured in a double-chambered well, where they were allowed to migrate, and penetrate the filter separating the chambers, to enter the lower chamber. After 24 hr of incubation, the number of cells attached to the lower side of the filter was counted. The IC_{50} values for moverastins A and B in this assay were 6.7 and 6.9 μg/ml, respectively (Figure 4B). Moverastins A and B did not show any cytotoxicity or growth inhibition after 72 hr toward EC17 cells, up to 10 μg/ml (data not shown).

Inhibition of FTase by Moverastins A and B In Vitro

Among cylindrol family compounds, cylindrol A and LL-Z1272ϵ were reported to be inhibitors of FTase [26]. Since moverastins A and B were determined to be cylindrol compounds, we examined whether they have an inhibitory effect on FTase. For this assay, FTase was partially purified from EC17 cells, and recombinant GST-H-Ras and [^{3}H]-farnesyl pyrophosphate were used as the substrates. As shown in Figures 5A and 5B, moverastins A and B inhibited FTase in a dose-dependent manner. With our assay system, the IC_{50} values of moverastins A and B were 6.8 and 7.5 μg/ml, respectively. Kinetic analysis revealed that the inhibitory pattern on the Lineweaver-Burk plot of moverastin A versus H-Ras was typical of noncompetitive inhibition, in which each line met together on the *x* axis, as shown in Figure 5C. From the Dixon plot analysis, the K_i value of moverastin A against FTase was found to be about 5.5 μg/ml, as shown in Figure 5D. The inhibitory pattern of moverastin B versus H-Ras was also noncompetitive (data not shown). In contrast, moverastins A and B did not show any inhibitory activity against GGTase up to 10 μg/ml, as judged from the amount of [^{3}H]-GGPP bound to GST-Rho A (Figures 5A and 5B).

Moverastins A and B Inhibit Migration of EC17 Cells by Inhibiting FTase

The findings that moverastins A and B inhibited the migration of EC17 cells, and were potential FTase inhibitors, led us to investigate whether the inhibition of cell migration is due to the suppression of H-Ras activation caused by the inhibition of FTase. First, we examined the expression of H-Ras in cultured EC17 cells. EC17 cells displayed relatively high levels of H-Ras protein compared with other human tumor cells (see Figure S1). The biochemical fractionation experiments revealed that H-Ras was much more prominent in the membrane fraction in EC17 cells (Figure 6A). However, treatment of cells with 10 μg/ml of moverastin A reduced the amount of H-Ras in the membrane fraction, which led to an increase in cytosolic H-Ras, indicating that moverastin A inhibited the activation of H-Ras by inhibiting the membrane localization through the inhibition of FTase in EC17 cells. The same procedure was carried out to detect the localization of N-Ras. However, the same concentration of moverastin A failed to inhibit the membrane localization of N-Ras (Figure 6A). Similar results were obtained when moverastin B was used (data not shown). Because the

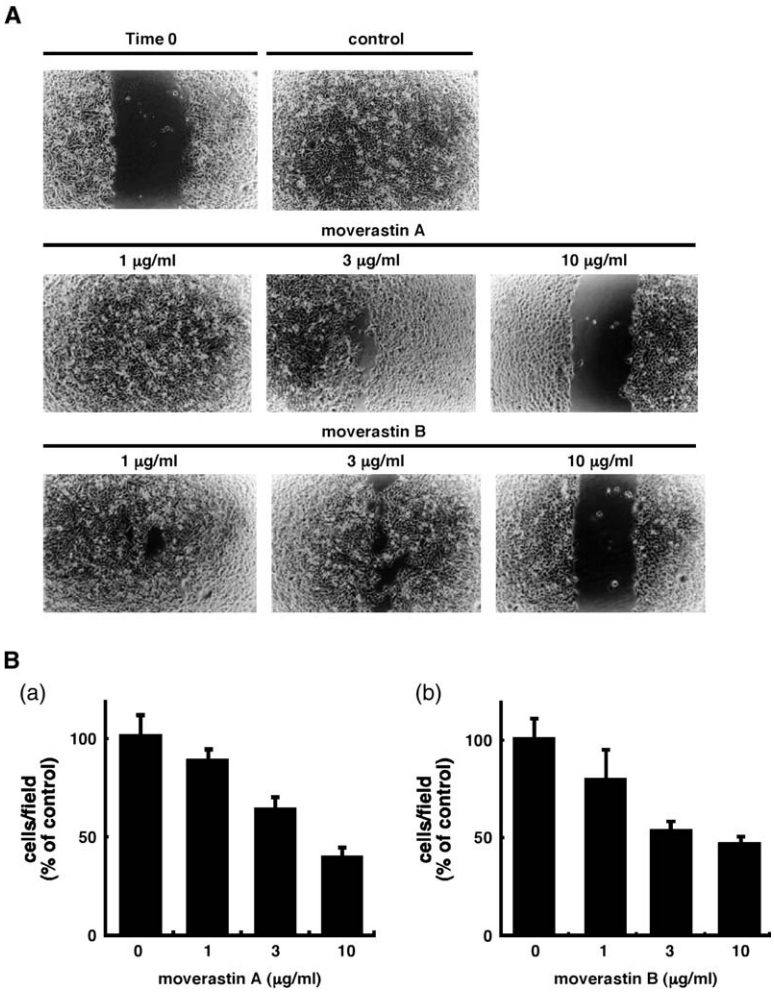

Figure 4. Effect of Moverastins A and B on Migration in EC17 Cells

(A) Wounding was introduced into confluent cultures of EC17 cells, as described in Experimental Procedures. The cells were incubated with various concentrations of moverastin A or moverastin B.

(B) EC17 cells were incubated with various concentrations of moverastin A (a) or moverastin B (b) in the top chamber for 24 hr. Then, the number of cells that migrated through the filter to the lower surface was counted. The results are the mean ± SD of five different fields.

activation of H-Ras is reported to further activate the PI3K/Akt pathway [17–19], we examined the effect of moverastin A on the phosphorylation of Akt. Moverastin A inhibited the level of phosphorylated Akt with the same dose range that inhibited the migration of EC17 cells (Figure 6B). In contrast, the same dose range of moverastin A did not affect the levels of phosphorylated Erk1/2, regulated by K- or N-Ras through the Raf/MEK pathway. Similar results were obtained when moverastin B was used (data not shown). The involvement of these pathways in the motility of EC17 cells was examined with a known inhibitor for each pathway. A PI3K inhibitor, LY294002, inhibited the migration of EC17 cells under conditions in which LY294002 inhibited the phosphorylation of Akt (Figures 6C and 6D). However, U0126, an inhibitor of MEK, did not inhibit the migration of EC17 cells, in spite of the disappearance of phosphorylated Erk1/2.

Discussion

In the course of screening for inhibitors of tumor cell migration, we obtained moverastin from the culture broth of *Aspergillus* sp. F7720. Although our present studies suggest that moverastin is a mixture of two diastereomers at the C-10 secondary allylic alcohol, the structure of each diastereomer (moverastins A and B) was determined in this mixture by spectroscopic analysis, because the separation of each diastereomer by HPLC was unsuccessful. The possibility that natural moverastin is a mixture of two diastereomers at C-10 was confirmed by chemical synthesis of moverastin as a diastereomeric mixture and by analysis of its NMR data. The preparation of each diastereomer by chemical synthesis revealed that moverastin A is a (10*R*)-isomer, and moverastin B is a (10*S*)-isomer, and they are members of the cylindrol family. Although several cyclindrols and their synthetic analogs have been reported, moverastins A and B are unique in having an exomethylene moiety in their structures (Figures 1A and 1B). Both moverastins had similar inhibitory effects on cell migration (Figures 4A and 4B). Therefore, we concluded that the configuration of C-10 had no effect on the inhibitory activity of moverastins A and B toward cell migration.

We also demonstrated that moverastins A and B inhibited FTase (Figures 4 and 5A); the inhibitory effects are specific to FTase, because they did not inhibit GGTase. Moreover, moverastins A and B inhibited FTase and cell migration with almost the same dose range and with the same inhibitory profile (Figures 4 and 5A). In addition, inhibitory patterns of moverastins A and B are noncompetitive with H-Ras (Figure 5C). These results correlated with the previously reported FTase inhibitory pattern of LL-Z1272ϵ, another cylindrol family compound, which was also reported to be

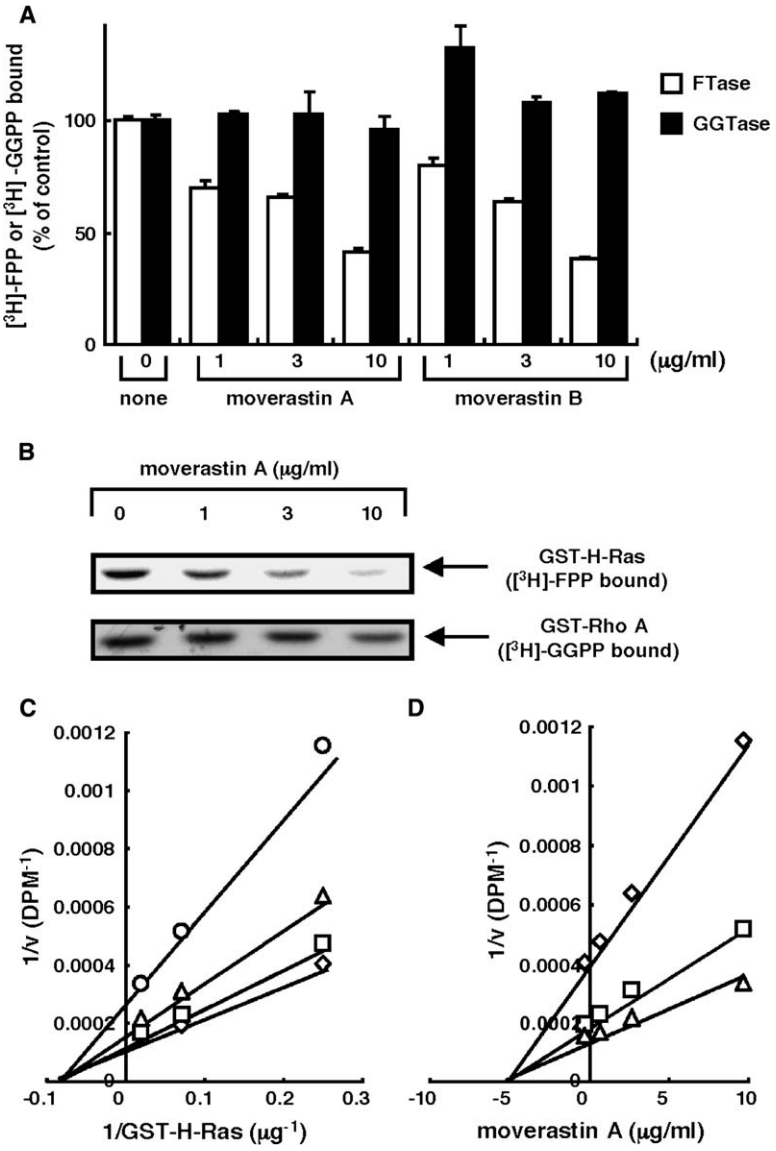

Figure 5. Effect of Moverastins A and B on FTase In Vitro

(A) Partially purified enzymes from EC17 cells were incubated with [^{3}H]-FPP plus recombinant GST-H-Ras for FTase assay or [^{3}H]-GGPP plus recombinant GST-Rho A for GGTase assay in the presence or absence of moverastin A or moverastin B. The reaction was terminated by the addition of TCA. The radioactivity of the TCA-insoluble fraction was measured. The results are the mean ± SD of four independent experiments.

(B) Partially purified enzymes from EC17 cells were incubated with [^{3}H]-FPP plus recombinant GST-H-Ras for FTase assay or [^{3}H]-GGPP plus recombinant GST-Rho A for GGTase assay in the presence or absence of moverastin A. The reaction was terminated by adding SDS sample buffer, and the product solution was subjected to SDS-PAGE and analyzed by autoradiography.

(C) Lineweaver-Burk plot of initial velocity versus GST-H-Ras concentration. Moverastin A concentrations are 0 (rhombus), 1 (square), 3 (triangle), and 10 (circle) μg/ml, respectively.

(D) Dixon plot of initial velocity versus moverastin A concentration. GST-H-Ras concentrations are 65 (rhombus), 217 (square), and 650 (triangle) μg/ml, respectively.

noncompetitive with Ras-peptide (Ras-CVLS) [26]. Because moverastins A and B inhibited FTase with similar potencies, the configuration of C-10 had no effect on the inhibitory activity against FTase.

It had not yet been reported that FTase-inhibiting cylindrols suppress protein farnesylation in a cultured cell system. Therefore, we examined whether moverastins A and B could inhibit protein farnesylation in EC17 cells. Moverastins A and B inhibited the membrane localization of H-Ras in EC17 cells, suggesting that they could inhibit the farnesylation of H-Ras in the cultured cell (Figure 6A). By contrast, they did not inhibit the membrane localization of N-Ras (Figure 6A). The difference can be explained by the finding that FTase inhibitors SCH 44342 and SCH 56582 inhibit the prenylation of H-Ras, but not of N-Ras [33]. In addition, while H-, K-, and N-Ras are substrates for FTase in vitro, K- and N-Ras, but not H-ras, are also substrates for GGTase [34]. Thus, K- and N-Ras are geranylgeranylated by GGTase in cells when FTase is inhibited. Therefore, it is likely that N-Ras is normally farnesylated in EC17 cells, however, it may be subjected to geranylgeranylation by GGTase in moverastin A- or B-treated EC17 cells, thereby retaining the ability to translocate to the membrane. Thus, our findings suggest that moverastins A and B could inhibit FTase, but not GGTase, in the cultured cell.

Among human tumor cells tested, EC17 cells showed high migrative capacity (data not shown) and a high level of farnesylated H-Ras protein. It has been reported that motility in human breast epithelial cells was induced by H-Ras, but not by N-Ras [35]. We similarly found that overexpression of H-Ras in NIH3T3 cells induced migration (data not shown). Taken together, expression of activated H-Ras at a high level seems to be responsible for the migrative capacity of EC17 cells. Because the dose of moverastins A and B required to inhibit the membrane localization of H-Ras is consistent with that for the inhibition of cell migration in EC17 cells, inhibition of the migration of EC17 cells by moverastin A or B was solely due to the inhibition of H-Ras farnesylation.

Although H-, K-, and N-Ras share many common signaling pathways leading to similar cellular responses,

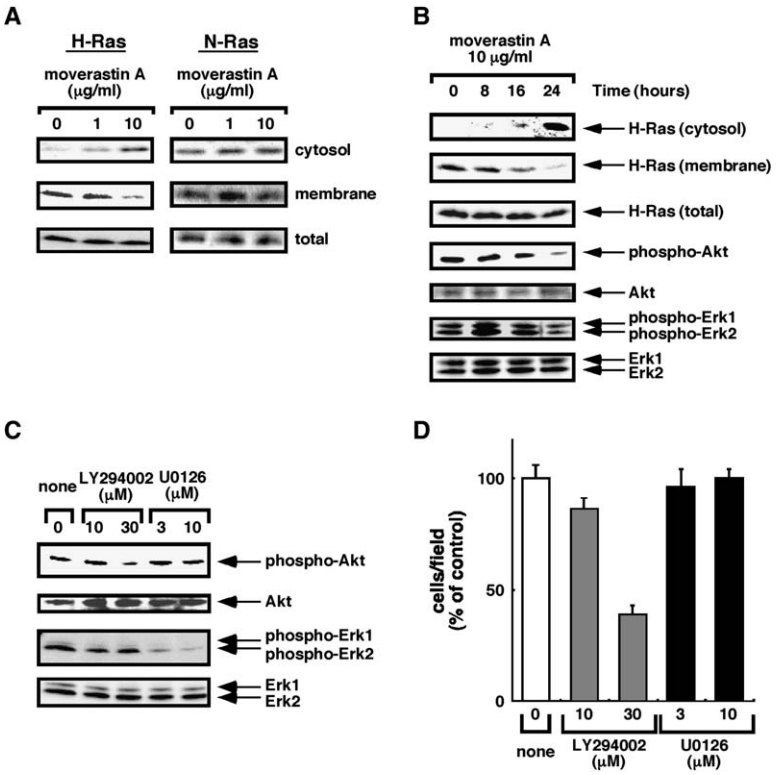

Figure 6. Effect of Moverastin A on H-Ras Translocation in EC17 Cells

(A) EC17 cells were incubated with moverastin A for 24 hr. Proteins were extracted and separated into cytosolic and membrane fractions, and then H- or N-Ras were detected by immunoblotting as described in Experimental Procedures. Total cell lysate was immunoblotted with anti-H-Ras or anti-N-Ras antibody.

(B) EC17 cells were incubated with 10 μg/ml of moverastin A for the periods indicated. H-Ras in cytosolic and membrane fractions was detected by immunoblotting as described in Experimental Procedures. Total cell lysate was immunoblotted with anti-H-Ras, anti-phospho-Akt, anti-Akt, anti-phospho-Erk, or anti-Erk antibody. The data shown are representative of three independent experiments.

(C) EC17 cells were incubated with the indicated concentrations of LY294002 or U0126 for 24 hr. Then, cells were collected, total cell lysate was prepared, and equal amounts of lysate were examined by Western blotting using anti-phospho-Akt, anti-Akt, anti-phospho-Erk, or anti-Erk antibody.

(D) EC17 cells were incubated with the indicated concentrations of LY294002 or U0126 in the top chamber for 24 hr. The cells that migrated through the filter to the lower surface were counted. The results are the mean ± SD of five different fields.

studies abroad clearly demonstrate unique roles for these three Ras. Unique functions of the Ras family members at the molecular level are supported by the demonstration that there are differences in the signal transduction pathways induced by Ras proteins. K- and N-Ras preferentially regulate the Raf/MEK/Erk pathway, and H-Ras mainly regulates the PI3K/Akt pathway [36–38]. Our finding that moverastins A and B inhibited the PI3K/Akt pathway, but not the Raf/MEK/Erk pathway (Figure 6B), indicated that moverastins A and B inhibited signal transduction downstream of H-Ras, selectively.

The contribution of the Raf/MEK/Erk pathway and PI3K/Akt pathway to cell migration differs with the cell line or stimulation. For example, the Raf/MEK/Erk pathway is necessary in the induction of cell migration by HGF in Madin-Darby canine kidney epithelial cells [17]. On the other hand, insulin-like growth factor 1-stimulated melanoma cell migration required the PI3K/Akt pathway, but not Raf/MEK/Erk pathway [39]. Because the migration of EC17 cells was suppressed by an inhibitor of the PI3K/Akt pathway, but not by an inhibitor of the Raf/MEK/Erk pathway (Figures 6C and 6D), it appears that the PI3K/Akt pathway dominantly regulates migration in EC17 cells. Taken together, our findings suggest that moverastins A and B inhibited the migration of EC17 cells by inhibiting the PI3K/Akt pathway through suppression of H-Ras farnesylation.

Significance

Despite significant advances in understanding the fundamental aspects of cancer, the development of metastatic lesions remains the predominant cause of death for most cancer patients. Cell migration is a crucial event in the spread of cancer and, consequently, the metastatic process. This prompted us to develop inhibitors of tumor cell migration as antimetastatic drugs. Because microbial products display diverse structures and unique activities, we have screened for inhibitors of tumor cell migration of microbial origin. As a result, we obtained a compound, moverastin, which belongs to the cylindrol family, from *Aspergillus* sp. F7720. Among the cylindrol family, moverastin is unique in having an exomethylene moiety at position C-11. However, an analysis by NMR spectroscopy raised the possibility that moverastin is a mixture of two diastereomers. This was proved by an analysis of a synthesized mixture of the two diastereomers. Each synthetic diastereomer (moverastin A and moverastin B) inhibited cell migration with similar potency. Furthermore, both diastereomers displayed similar inhibitory activities for FTase in vitro, indicating that the configuration of C-10 did not affect the inhibitory activity for either cell migration or FTase. Our findings demonstrate that moverastins A and B inhibited the migration of tumor cells by inhibiting farnesylation of H-Ras, and subsequent H-Ras-dependent activation of the PI3K/Akt pathway. In this study, we found an effect of the cylindrol family on cultured tumor cells. The combination of a chemical approach and a cell biological approach enabled us to determine the structure of moverastin and to examine the structure-activity relationship and the biological function of moverastins A and B in vitro and in vivo. We are currently synthesizing moverastin derivatives, the structures of which are based on our findings on the structure-activity

relationship, and the biological activities of the derivatives are under investigation.

Experimental Procedures

Materials

LY294002 and U0126 were purchased from Sigma Chemical Co. (St. Louis, MO). Polyclonal antibody against H-Ras and polyclonal antibody against N-Ras were purchased from Santa Cruz Biotechnology (Santa Cruz, CA). Phospho-Akt (Ser473) antibody, Akt antibody, phospho-p44/42 MAP kinase Erk1/2 (Thr202/Tyr204) antibody, and p44/42 MAP kinase Erk1/2 antibody were purchased from Cell Signaling Technology, Inc. (Beverly, MA).

Cell Culture

Human tumor cells, including EC17 cells, were grown in RPMI 1640 medium containing 5% fetal bovine serum (FBS).

Synthesis of Moverastin

(6″R,7″R,8″R)-3-Chloro-4,6-dihydroxy-2-methyl-5-[3′-methyl-5-(6″,7″,8″-trimethyl-1″,4″-dioxaspiro[4.5]dec-7″-yl)penta-2′,4′-dienyl]benzaldehyde (4)

A mixture of ascochlorin (**3**, 0.013 g, 0.32 mmol), ethylene glycol (0.40 g, 6.4 mmol), and *p*-toluene sulfonic acid (6.0 mg, 0.032 mmol) in toluene (8 ml) was heated and refluxed through a column of MS 4A under slightly reduced pressure (bath temperature: 70ºC) for 3 hr. The reaction mixture was poured into a saturated $NaHCO_3$ solution and extracted three times with ether. The combined ether solution was washed with water and the saturated NaCl solution, dried with Na_2SO_4, and concentrated in vacuo. Column chromatography (SiO_2) of the residue afforded **4** (0.17 g, quantity). See Supplemental Data for further details.

(6′R,7′S,8′R)-4-(6′,7′,8′-Trimethyl-1′,4′-dioxaspiro[4.5]dec-7′-yl)-but-3-en-2-one (5)

Ozone was passed through a cooled and stirred solution of **4** (0.16 g, 0.35 mmol) in pyridine (0.75 ml) and CH_2Cl_2 (15 ml) at −78ºC until the mixture turned to yellowish green. After the removal of excess ozone by N_2 bubbling (15 min), Me_2S (0.5 ml, 6.8 mmol) was added dropwise to the mixture, and the temperature was raised gradually to room temperature. After stirring for 1 hr at room temperature, solvent was evaporated off and the residue was chromatographed on SiO_2, to give 0.086 g (99%) of **5** as a pale yellow oil. See Supplemental Data for further details.

(6′R,7′S,8′R)-4-(6′,7′,8′-Trimethyl-1′,4′-dioxaspiro[4.5]dec-7′-yl)butan-2-one (6)

A mixture of **5** (0.080 g, 0.32 mmol) and 10% Pd-C (33 mg) in EtOAc (5 ml) was stirred vigorously under H_2 at room temperature for 3 hr. After dilution of the mixture with EtOAc and filtration through Celite, the solvent was evaporated off, to give 0.084 g (quantity) of **6** as a colorless oil. See Supplemental Data for further details.

Trifluoromethanesulfonic Acid (6″R,7″S,8″R)-1-[2′-(6″,7″,8″-trimethyl-1″,4″-dioxaspiro[4.5]dec-7″-yl)ethyl]vinyl este (7)

To a cooled and stirred solution of **6** (0.059 g, 0.23 mmol) in dry THF (5 ml) was added, drop-wise, a solution of KHMDS (0.5 M in toluene, 0.75 ml, 0.37 mmol) under Ar at −78ºC. After stirring for 15 min at the same temperature, the resulting enolate was quenched by the addition 5-chloro-2-(*N,N*-bis[trifluoromethanesulfonyl]amino)pyridine (0.13 g, 0.35 mmol), and stirring was continued for 1 hr. A saturated $NaHCO_3$ solution was then added, and the resulting mixture was extracted three times with EtOAc. The combined organic phase was washed with water and the saturated NaCl solution, dried (Na_2SO_4), and concentrated in vacuo. The residue was chromatographed on SiO_2 to give 0.057 g (64%) of **7**. See Supplemental Data for further details.

2-Allyl-1,3-bis(methoxymethoxy)-5-methylbenzene (9)

To a solution of **8** (6.37 g, 0.03 mol) and TMEDA (9 ml, 0.06 mol) in dry THF (100 ml) was added *n*-BuLi (1.56 M in *n*-hexane, 23 ml, 0.036 mol) at −20ºC. After 1.5 hr, allyl bromide (5.2 ml, 0.06 mol) was added to the mixture at −20ºC, and stirring was continued overnight at room temperature. The solvent was evaporated off, and the residue was diluted with ether and washed with water and a saturated NaCl solution. Drying on Na_2SO_4 and evaporation gave a crude product, which was purified by column chromatography (SiO_2) to give 4.54 g (60%) of **9** as a colorless oil. See Supplemental Data for further details.

3-Allyl-2,4-bis(methoxymethoxy)-6-methylbenzaldehyde (10)

To a solution of **9** (2.07 g, 8.2 mmol) and TMEDA (7.4 ml, 49 mmol) in dry ether (200 ml) was added *n*-BuLi (1.56 M in *n*-hexane, 15.8 ml, 25 mmol) at −20ºC. After 2 hr, DMF (1.0 ml, 60 mmol) was added to the mixture at −20ºC, and stirring was continued overnight at room temperature. The reaction mixture was diluted with ether and washed with water and a saturated NaCl solution. Drying on Na_2SO_4 and evaporation gave a crude product, which was purified by column chromatography (SiO_2) to give 0.63 g of starting material (**9**) and 0.868 g (54% based on recovery) of **10** as a colorless oil, which crystallized when placed in a refrigerator. See Supplemental Data for further details.

2,4-Bis(methoxymethoxy)-6-methyl-3-(2-oxoethyl)benzaldehyde (11)

Ozone was passed through a cooled (−78ºC) and stirred solution of **10** (0.293 g, 10.4 mmol) in CH_2Cl_2 (30 ml) until the solution turned pale blue. After the removal of excess ozone by N_2 bubbling (10 min), PhP_3 (0.301 g, 12.5 mmol) was added to the mixture, and the temperature was raised gradually to room temperature. The solvent was then evaporated off and the residue was chromatographed on SiO_2 to give 0.218 g (74%) of **11** as a colorless oil. See Supplemental Data for further details.

(6‴R,7‴S,8‴R)-3-{2′-Hydroxy-3′-[2″-(6‴,7‴,8‴-trimethyl-1‴,4‴-dioxaspiro[4.5]dec-7‴-yl)ethyl]but-3′-enyl}-2,4-bis(methoxymethoxy)-6-methylbenzaldehyde (12)

To a solution of $CrCl_2$ (44.0 mg, 0.148 mmol) and $NiCl_2$ (2.2 mg) in dry DMF (5 ml) was added a solution of **7** (14.4 mg, 0.0373 mmol) and **11** (21.0 mg, 0.0746 mmol) in dry DMF (5 ml) at room temperature. After 1 hr, the reaction mixture was poured into water and extracted three times with ether. The combined ether solution was washed with water and a saturated $NaHCO_3$ solution, dried (Na_2SO_4), and concentrated in vacuo. Purification of the crude product by column chromatography (SiO_2) gave **12** (12.0 mg, 62%) as a colorless oil. See Supplemental Data for further details.

Moverastin

To a solution of **12** (18.1 mg, 0.0347 mmol) in THF (0.5 ml) was added concentrated HCl (0.2 ml), and the resulting mixture was stirred at room temperature for 30 min. After neutralization by the addition of a saturated $NaHCO_3$ solution, the mixture was extracted three times with EtOAc and the combined organic phase was washed with water and the saturated $NaHCO_3$ solution, dried (Na_2SO_4), and concentrated in vacuo. The residue was purified by column chromatography (SiO_2) to give 10.9 mg (82%) of moverastin as colorless crystals.

The NMR data on our synthetic moverastin were identical with those on natural moverastin.

Separation of 10-Epimers of Moverastin

(S)-MTPA Esters of 12 ([10R]- and [10S]-13). To a stirred solution of **12** (48.4 mg, 0.093 mmol) and DMAP (34 mg, 0.279 mmol) in dry CH_2Cl_2 (5 ml) was added (*R*)-MTPACl (35 μl, 0.186 mmol) under Ar at 0ºC. After 1 hr, the reaction was quenched by the addition of a saturated $NaHCO_3$ solution and the product was extracted three times with ether. The combined ether solution was washed with water and the saturated NaCl solution, dried (Na_2SO_4), and concentrated in vacuo to afford a crude product. Purification by column chromatography (SiO_2) gave a diastereomeric mixture of **13** (54.0 mg, 81%). See Supplemental Data for further details.

Two 10-epimers were separated by preparative HPLC (SiO_2, solvent system: hexane-EtOAc [6:1]) and 26 mg of (10*R*)-**13** and 26 mg of (10*S*)-**13** were obtained. See Supplemental Data for further details.

(R)-MTPA Esters of 12. In the same manner as described for the preparation of (10*R*)- and (10*S*)-**13**, (*R*)-MTPA esters of moverastin were obtained in 82% yield (10.9 mg) from 11 mg of **12**, two isomers of which were separated by preparative HPLC to afford (10*S*)- and (10*R*)-isomers (5 mg each). See Supplemental Data for further details.

(10R)-Moverastin (1). To a stirred and ice-cooled solution of (10*R*)-**13** (27 mg, 0.037 mmol) in MeOH (0.5 ml) was added NaOMe (28% in MeOH, 0.5 ml). After 1 hr at the same temperature, the reaction mixture was neutralized by the addition of 3 N HCl and extracted three times with ether. The combined ether solution was washed

with a saturated $NaHCO_3$ solution, water, and the saturated NaCl solution, dried (Na_2SO_4), and concentrated in vacuo. The residue was chromatographed (SiO_2) to give a mixture of (10*R*)-**12** and partially deacetalized ketone. The mixture was deluted with THF (0.5 ml) and treated with concentrated HCl (0.2 ml) and worked-up as described for the preparation of (10*RS*)-moverastin, to give 10 mg (69%) of (10*R*)-moverastin as colorless crystals after chromatographic purification. See Supplemental Data for further details.

(10S)-Moverastin (2). In the same manner as described above, 8.9 mg (61%) of (10*S*)-moverastin was obtained from 27 mg of (10*S*)-**13**. See Supplemental Data for further details.

Wound Healing Assay

A confluent monolayer of EC17 cells (7.5×10^4 cells/well in a 48 well plate) was scratched with a white tip to create a cell-free zone in each well, about 1 mm in width. The medium was replaced with medium containing 1% FBS with or without of test sample. After 24 hr, cells were observed under the microscope.

Transwell Migration Assay

The chemotactic migration of cells was assayed in a chemotaxicell chamber (KURABO, Osaka, Japan) as previously reported, with some modifications [40]. The cells (3×10^5) suspended in medium containing 1% FBS were added to the upper compartment of the chamber, and were incubated with conditioned medium in the lower compartment for 24 hr. The filter was fixed with MeOH and stained with hematoxylin. The number of cells that migrated through the filter to the various areas of the lower surface was counted under the microscope.

Assay Methods for FTase and GGTase

To obtain FTase and GGTase, we used a modification of the method described by Omura et al. [41]. EC17 cells were lysed and centrifuged, and the supernatant was submitted to fractionation by ammonium sulfate. The ~30%–60%-saturated ammonium sulfate fraction was used as FTase and GGTase. cDNA corresponding to c-Ha-Ras, was isolated from EC17 cells using RT-PCR, and subcloned into pGEX-2T (Amersham Pharmacia Biotech, Tokyo, Japan). c-Ha-Ras protein was expressed in DH5α cells as a GST-fusion protein, and purified on glutathione-agarose beads (Sigma Chemical Co.). Fusion protein was used for the FTase assay as a substrate. Human Rho A cDNA was kindly provided by Dr. S. Narumiya (Kyoto University). The human Rho A cDNA was subcloned into pGEX-2T. Rho A protein was expressed in DH5α cells as a GST-fusion protein, and purified on glutathione-agarose beads. Fusion protein was used for the GGTase assay as a substrate.

To measure FTase and GGTase activity, we used a modification of the method described by Omura et al. [41]. The standard reaction mixture contained the following components in a final volume of 60 μl: 10 μg of partially purified enzymes from the cytosol of EC17 cells, 10 μg of recombinant GST-H-Ras protein for the FTase assay or 8 μg of recombinant GST-Rho A protein for the GGTase assay, 0.06 μM of [^{3}H]-FPP (596 GBq/mmol, New England Nuclear) for the FTase assay or 0.08 μM of [^{3}H]-GGPP (1.48 TBq/mmol, Amersham Bioscience) for the GGTase assay, 50 mM Tris-HCl (pH 7.5), 50 μM $ZnCl_2$, 4 mM $MgCl_2$ and 4 mM DTT. The reaction was initiated by addition of enzyme and incubated for 1 hr at 37ºC. The reaction was stopped by addition of 0.5 ml of 1% SDS in MeOH and 0.5 ml of 30% TCA. After vortexing, the tubes were left for 1 hr on ice. The mixture was then filtered on a Whatman GF/C filter, washed with 5 ml of 6% TCA using a Skatron cell harvester. The dried filter was finally placed in a liquid scintillation counter. A blank value was determined in a parallel incubation with boiled enzymes and was subtracted before calculating percent inhibition.

Separation of Plasma Membrane and Cytosolic Fractions

Cells were harvested and resuspended in buffer A (20 mM Hepes-KOH, pH 7.5, 10 mM KCl, 1.5 mM $MgCl_2$, 1 mM EDTA, 1mM EGTA, and 1mM DTT) containing 250 mM sucrose and a mixture of protease inhibitors (1 mM phenylmethylsulfonyl fluoride [PMSF], 1% aprotinin, 1 mM leupeptin, 1 μg/ml pepstatin A, and 1 μg/ml chymostatin). The cells were homogenized and unbroken cells were removed by centrifuging the homogenates at 1000 × g for 10 min at 4ºC. The supernatant was centrifuged at 100,000 × g for 1 hr at 4ºC to prepare the cytosolic fraction. Pellets were lysed in RIPA buffer at 4ºC with sonication. The lysates were centrifuged at 100,000 × g for 15 min at 4ºC to give the plasma membrane fraction.

Western Blotting

The cells were lysed in RIPA buffer at 4ºC with sonication. The lysates were centrifuged at 15,000 × g for 15 min, and the concentration of the protein in each lysate was determined with Coomassie brilliant blue G-250. Loading buffer (42 mM Tris-HCl, 10% glycerol, 2.3% SDS, 5% 2-mercaptoethanol, and 0.002% bromophenol blue) was then added to each lysate, which was subsequently boiled for 3 min and then electrophoresed on an SDS polyacrylamide gel. Proteins were transferred to Hybond-P membrane (Amersham Pharmacia Biotech) and immunoblotted with anti-H-Ras, anti-N-Ras, anti-phospho-Akt (Ser473), anti-Akt, anti-phospho-p44/42 MAP kinase Erk1/2 (Thr202/Tyr204), or anti-p44/42 MAP kinase Erk1/2 antibody. Detection was performed with enhanced chemiluminescence reagent (NEN Life Science Products, Boston, MA).

Supplemental Data

Supplemental Data including one figure are available at http://www.chembiol.com/cgi/content/full/12/12/1337/DC1/.

Acknowledgments

The authors are grateful to Dr. M. Matsumoto (Chugai Pharmaceutical Co. LTD) for the gift of ascochlorin. They also thank Dr. K. Dobashi (Mercian Co. LTD) for fermentation and taxonomic study of the produced strain. This study was partly supported by grants from the Ministry of Education, Culture, Sports, Science, and Technology of Japan.

Received: July 13, 2005
Revised: September 8, 2005
Accepted: September 29, 2005
Published: December 16, 2005

References

1. Condeelis, J. (2001). How is actin polymerization nucleated in vivo? Trends Cell Biol. *11*, 288–293.
2. Pollard, T.D., and Borisy, G.G. (2003). Cellular motility driven by assembly and disassembly of actin filaments. Cell *112*, 453–465.
3. Theriot, J.A., and Mitchison, T.J. (1991). Actin microfilament dynamics in locomoting cells. Nature *352*, 126–131.
4. Wear, M.A., Schafer, D.A., and Cooper, J.A. (2000). Actin dynamics: assembly and disassembly of actin networks. Curr. Biol. *10*, R891–R895.
5. Ridley, A.J. (1996). Rho: theme and variations. Curr. Biol. *6*, 1256–1264.
6. Qiu, R.G., Chen, J., McCormick, F., and Symons, M. (1995). A role for Rho in Ras transformation. Proc. Natl. Acad. Sci. USA *92*, 11781–11785.
7. Ridley, A.J., and Hall, A. (1992). The small GTP-binding protein rho regulates the assembly of focal adhesions and actin stress fibers in response to growth factors. Cell *70*, 389–399.
8. Ridley, A.J., Comoglio, P.M., and Hall, A. (1995). Regulation of scatter factor/hepatocyte growth factor responses by Ras, Rac, and Rho in MDCK cells. Mol. Cell. Biol. *15*, 1110–1122.
9. Nobes, C.D., and Hall, A. (1995). Rho, rac, and cdc42 GTPases regulate the assembly of multimolecular focal complexes associated with actin stress fibers, lamellipodia, and filopodia. Cell *81*, 53–62.
10. Fox, P.L., Sa, G., Dobrowolski, S.F., and Stacey, D.W. (1994). The regulation of endothelial cell motility by p21 ras. Oncogene *9*, 3519–3526.
11. Klemke, R.L., Leng, J., Molander, R., Brooks, P.C., Vuori, K., and Cheresh, D.A. (1998). CAS/Crk coupling serves as a "molecular switch" for induction of cell migration. J. Cell Biol. *140*, 961–972.
12. Nobes, C.D., and Hall, A. (1999). Rho GTPases control polarity, protrusion, and adhesion during cell movement. J. Cell Biol. *144*, 1235–1244.
13. Hancock, J.F., Paterson, H., and Marshall, C.J. (1990). A polybasic domain or palmitoylation is required in addition to the

CAAX motif to localize p21ras to the plasma membrane. Cell *63*, 133–139.
14. Marshall, C.J. (1996). Ras effectors. Curr. Opin. Cell Biol. *8*, 197–204.
15. Klemke, R.L., Cai, S., Giannini, A.L., Gallagher, P.J., de Lanerolle, P., and Cheresh, D.A. (1997). Regulation of cell motility by mitogen-activated protein kinase. J. Cell Biol. *137*, 481–492.
16. Nguyen, D.H., Catling, A.D., Webb, D.J., Sankovic, M., Walker, L.A., Somlyo, A.V., Weber, M.J., and Gonias, S.L. (1999). Myosin light chain kinase functions downstream of Ras/ERK to promote migration of urokinase-type plasminogen activator-stimulated cells in an integrin-selective manner. J. Cell Biol. *146*, 149–164.
17. Tanimura, S., Nomura, K., Ozaki, K., Tsujimoto, M., Kondo, T., and Kohno, M. (2002). Prolonged nuclear retention of activated extracellular signal-regulated kinase 1/2 is required for hepatocyte growth factor-induced cell motility. J. Biol. Chem. *277*, 28256–28264.
18. Rodriguez-Viciana, P., Warne, P.H., Vanhaesebroeck, B., Waterfield, M.D., and Downward, J. (1996). Activation of phosphoinositide 3-kinase by interaction with Ras and by point mutation. EMBO J. *15*, 2442–2451.
19. Pacold, M.E., Suire, S., Perisic, O., Lara-Gonzalez, S., Davis, C.T., Walker, E.H., Hawkins, P.T., Stephens, L., Eccleston, J.F., and Williams, R.L. (2000). Crystal structure and functional analysis of Ras binding to its effector phosphoinositide 3-kinase gamma. Cell *103*, 931–943.
20. Keely, P.J., Westwick, J.K., Whitehead, I.P., Der, C.J., and Parise, L.V. (1997). Cdc42 and Rac1 induce integrin-mediated cell motility and invasiveness through PI(3)K. Nature *390*, 632–636.
21. Bourne, H.R., Sanders, D.A., and McCormick, F. (1990). The GTPase superfamily: a conserved switch for diverse cell functions. Nature *348*, 125–132.
22. Desrosiers, R.R., Cusson, M.H., Turcotte, S., and Beliveau, R. (2005). Farnesyltransferase inhibitor SCH-66336 downregulates secretion of matrix proteinases and inhibits carcinoma cell migration. Int. J. Cancer *114*, 702–712.
23. Kusama, T., Mukai, M., Tatsuta, M., Matsumoto, Y., Nakamura, H., and Inoue, M. (2003). Selective inhibition of cancer cell invasion by a geranylgeranyltransferase-I inhibitor. Clin. Exp. Metastasis *20*, 561–567.
24. Lauffenburger, D.A., and Horwitz, A.F. (1996). Cell migration: a physically integrated molecular process. Cell *84*, 359–369.
25. Liotta, L.A. (1986). Tumor invasion and metastases—role of the extracellular matrix: Rhoads Memorial Award lecture. Cancer Res. *46*, 1–7.
26. Singh, S.B., Ball, R.G., Bills, G.F., Cascales, C., Gibbs, J.B., Goetz, M.A., Hoogsteen, K., Jenkins, R.G., Liesch, J.M., Lingham, R.B., et al. (1996). Chemistry and biology of cylindrols: novel inhibitors of ras farnesyl-protein transferase from *Cylindrocarpon lucidum*. J. Org. Chem. *61*, 7727–7737.
27. Comins, D.L., and Dehghani, A. (1992). Pyridine-Derived Triflating Reagents: an improved preparation of vinyl triflates from metallo enolates. Tetrahedron Lett. *33*, 6299–6302.
28. Ohta, S., Nozaki, A., Ohashi, N., Matsukawa, M., and Okamoto, M. (1988). A total synthesis of grifolin. Chem. Pharm. Bull. (Tokyo) *36*, 2239–2243.
29. Takai, K., Kimura, K., Kuroda, T., Hiyama, T., and Nozaki, H. (1983). Selective Grignard-type carbonyl addition of alkenyl halides mediated by chromium (Ii) chloride. Tetrahedron Lett. *24*, 5281–5284.
30. Takai, K., Tagashira, M., Kuroda, T., Oshima, K., Utimoto, K., and Nozaki, H. (1986). Reactions of alkenylchromium reagents prepared from alkenyl trifluoromethanesulfonates (triflates) with chromium(Ii) chloride under nickel catalysis. J. Am. Chem. Soc. *108*, 6048–6050.
31. Ohtani, I., Kusumi, T., Kashman, Y., and Kakisawa, H. (1991). High-field Ft NMR application of Mosher method: the absolute-configurations of marine terpenoids. J. Am. Chem. Soc. *113*, 4092–4096.
32. Nakae, K., Yoshimoto, Y., Sawa, T., Homma, Y., Hamada, M., Takeuchi, T., and Imoto, M. (2000). Migrastatin, a new inhibitor of tumor cell migration from *Streptomyces* sp. MK929–43F1: taxonomy, fermentation, isolation and biological activities. J. Antibiot. (Tokyo) *53*, 1130–1136.
33. Zhang, F.L., Kirschmeier, P., Carr, D., James, L., Bond, R.W., Wang, L., Patton, R., Windsor, W.T., Syto, R., Zhang, R., et al. (1997). Characterization of Ha-ras, N-ras, Ki-Ras4A, and Ki-Ras4B as in vitro substrates for farnesyl protein transferase and geranylgeranyl protein transferase type I. J. Biol. Chem. *272*, 10232–10239.
34. Lerner, E.C., Qian, Y., Hamilton, A.D., and Sebti, S.M. (1995). Disruption of oncogenic K-Ras4B processing and signaling by a potent geranylgeranyltransferase I inhibitor. J. Biol. Chem. *270*, 26770–26773.
35. Kim, M.S., Lee, E.J., Kim, H.R., and Moon, A. (2003). p38 kinase is a key signaling molecule for H-Ras-induced cell motility and invasive phenotype in human breast epithelial cells. Cancer Res. *63*, 5454–5461.
36. Yan, J., Roy, S., Apolloni, A., Lane, A., and Hancock, J.F. (1998). Ras isoforms vary in their ability to activate Raf-1 and phosphoinositide 3-kinase. J. Biol. Chem. *273*, 24052–24056.
37. Voice, J.K., Klemke, R.L., Le, A., and Jackson, J.H. (1999). Four human ras homologs differ in their abilities to activate Raf-1, induce transformation, and stimulate cell motility. J. Biol. Chem. *274*, 17164–17170.
38. Li, W., Zhu, T., and Guan, K.L. (2004). Transformation potential of Ras isoforms correlates with activation of phosphatidylinositol 3-kinase but not ERK. J. Biol. Chem. *279*, 37398–37406.
39. Neudauer, C.L., and McCarthy, J.B. (2003). Insulin-like growth factor I-stimulated melanoma cell migration requires phosphoinositide 3-kinase but not extracellular-regulated kinase activation. Exp. Cell Res. *286*, 128–137.
40. Saiki, I., Murata, J., Yoneda, J., Kobayashi, H., and Azuma, I. (1994). Influence of fibroblasts on the invasion and migration of highly or weakly metastatic B16 melanoma cells. Int. J. Cancer *56*, 867–873.
41. Omura, S., Van der Pyl, D., Inokoshi, J., Takahashi, Y., and Takeshima, H. (1993). Pepticinnamins, new farnesyl-protein transferase inhibitors produced by an actinomycete: I. Producing strain, fermentation, isolation and biological activity. J. Antibiot. (Tokyo) *46*, 222–228.

Accession Numbers

The strain *Aspergillus* sp.F7720 has been deposited in the National Institute of Advanced Industrial Science and Technology, Tsukuba, Japan, with accession number FERM P-18198.